CHAPTER 4

THE PROPOSED MAXIMUM CONSTANT D_0 CONTROL STRATEGY

4.1 Introduction

In the previous chapter, a constant equivalent duty ratio control strategy is proposed for the seven-active-switch boostbuck rectifier to achieve bidirectional power flow capability. In addition, based on the closed form duty ratio functions, both DC and small models of the proposed converter are also derived. It is found that for a given output the constant D_0 control is not unique. A natural question is " what is the optimal one? ". From the DC model one can see that $V_O=D_0V_C$. Hence, from the viewpoint of practical application, it is a nice policy to choose maximum D_0 control. Normally, the seven active switches operate randomly so as to reduce the resulting control, it is rather difficult to predict the dynamic behavior of the new converter. Fortunately, the analytic result and the derived averaged model of the previous chapter provide one excellent tool to find the solution of maximum constant D_0 control. The detailed derivation process will be given in this chapter. Also, an equivalent circuit model of the proposed converter is also derived for convenient application while making analysis, simulation and design. Finally, some

experimental results are also provided for demonstrating the validity of the proposed maximum constant D_0 control strategy.

4.2 The Distributed D_0 Control Strategy

For convenient reference, the basic circuit topology of the proposed three-phase bidirectional step-up/down converter is repeated in Fig. 4.1, where $S_1, S_2, \ldots, S_7$ are active switches and R_S is the ESR of inductor L_S.

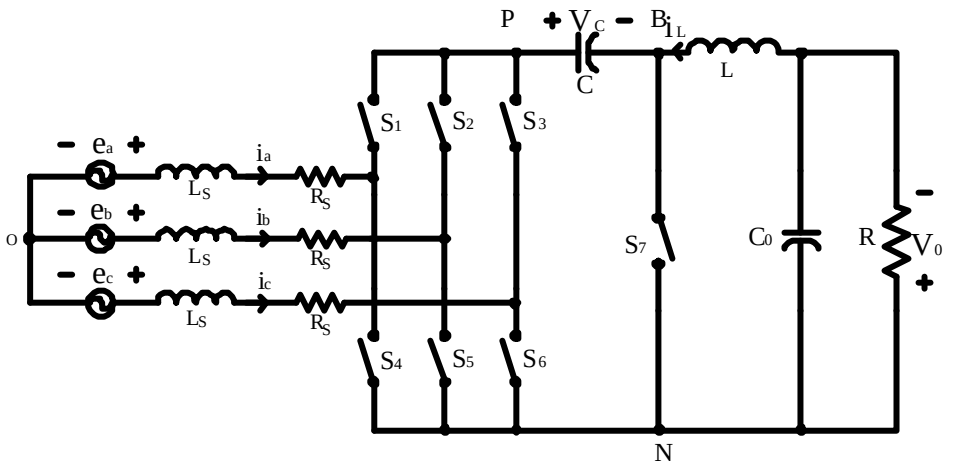

Fig. 4.1 Power circuit of the bidirectional three phase step-up/down converter

From Fig. 4.1 one can see that if S_7 is turned on then the subcircuit to the left of BN branch is a familiar three-phase boost rectifier without the load parallelled with capacitor C. Similarly, if switches S_i, $i = 1, 2, \ldots, 7$ are operated such that V_{PN} is short circuited whenever V_{BN} is opened and vice versa, then the subcircuit to the right of PN branch is basically a buck dc converter. However, unlike the boost

ac/dc converter where the upper and the lower switches of each bridge arm are not allowed to be shorted, switches S_i, $i = 1, 2, \ldots, 6$ can be operated independently. In fact, a generalized zero voltage space vectors concept was proposed to integrate the ac subcircuit and the dc subcircuit to achieve ideal AC/DC converter characteristic in [12, 42]. From [42], all six switches in three bridge arms are turned on for transferring the stored energy in capacitor C to the dc output to achieve better efficiency. Just like C'uk converter operation principle, during this period, switch S_7 is open circuited. Similarly, when S_7 is short circuited, the subcircuit to the left of line BN can be operated as a boost ac/dc converter with bidirectional power flow capability to achieve constant dc voltage across C [44]. From Fig. 4.1, due to use of a controllable active switch (S_7), the AC/DC converter can now be operated with reverse power flow. Also, from the output stage, one can see that to achieve a constant dc voltage, it is required to have an equivalent dc duty ratio for S_7. In [12, 42], the switching signals were determined from the current errors and the equivalent dc duty ratio of S_7 is time varying. The random switching behavior of all active switches renders the derivation of a dynamic model almost impossible. In the next section, a closed form duty ratio control law for achieving the ideal performance is derived. First, denote d_k, $k = 1, 2, \ldots, 7$ as the duty ratio of S_k in Fig. 4.1. Then, with a view to achieving a constant d_7 and integrating the ac and dc subcircuits by using

the generalized zero voltage space vectors as [12, 42] for the proposed PWM control, Fig. 4.2 shows a gating signal pattern for the seven active witches in one switching period.

Thus, from Fig. 4.2 one can see that for the switches located at the upper three bridge arms, there is a period called $d_{01}T_S$ (corresponding to a portion of $(d_2 - \frac{d_0}{2})T_S$ in Fig. 4.2) where only S_k, $k = 1, 2, 3$ are turned on. Similarly, for the lower three bridge arms, there is a period, called $d_{02}T_S$ (corresponding to a portion of $(d_6 - \frac{d_0}{2})T_S$ in Fig. 4.2) where only S_{k+3}, $k = 1, 2, 3$ are all turned on. Finally, when S_7 is open circuited, all six bridge switches are turned on for a period of d_0T_S $(= \frac{1}{2}d_0T_S + \frac{1}{2}d_0T_S)$. Hence, from Fig. 4.2 one has

$$d_0 + d_7 = 1, \text{ and}$$

$$d_k + d_{k+3} = 1 + d_0, \quad k = 1, 2, 3. \tag{4.1}$$

In summary, the proposed distributed constant D_0 control strategy distribute one half of D_0T_S to beginning of T_S and the other half to the end of T_S as can be observed clearly from Fig. 4.2.

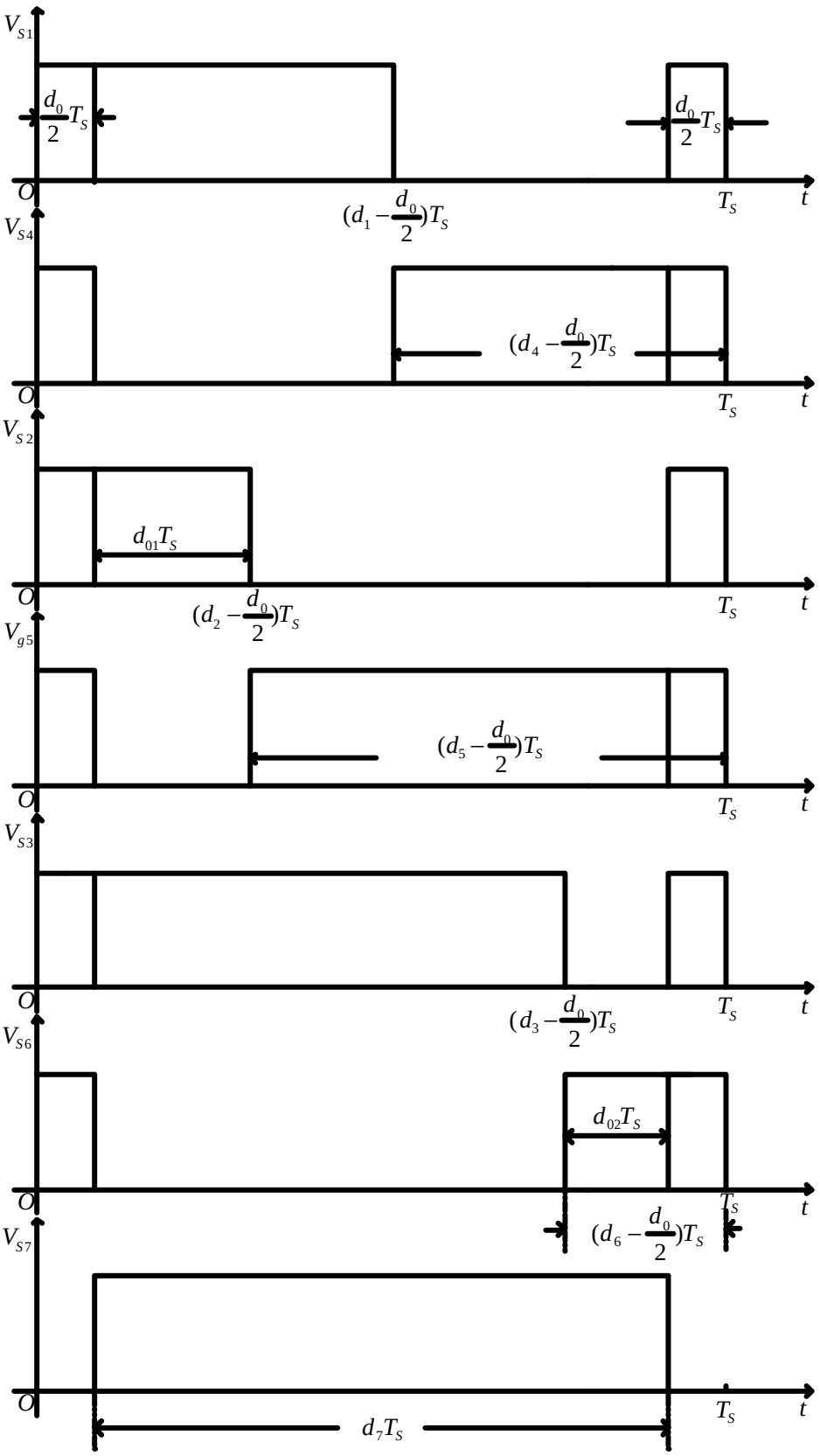

Fig. 4.2 Gating signal pattern for seven switches

4.3 Derivation of Equivalent Circuit Model

Assume that the switching frequency of the active switches is much higher than the ac line frequency. Then, one can apply the familiar state space averaging technique [43] to get the following averaged equations

$$L_S \frac{di_a}{dt} = -R_S i_a + \frac{1}{3}(-2d_1 + d_2 + d_3)v_C + e_a \tag{4.2}$$

$$L_S \frac{di_b}{dt} = -R_S i_b + \frac{1}{3}(d_1 - 2d_2 + d_3)v_C + e_b \tag{4.3}$$

$$L_S \frac{di_c}{dt} = -R_S i_c + \frac{1}{3}(d_1 + d_2 - 2d_3)v_C + e_c \tag{4.4}$$

$$L \frac{di_L}{dt} = (1 - d_7)v_C - v_O \tag{4.5}$$

$$C \frac{dv_C}{dt} = d_1 i_a + d_2 i_b + d_3 i_c - (1 - d_7)i_L \tag{4.6}$$

$$C_O \frac{dv_O}{dt} = i_L - \frac{1}{R}v_O \tag{4.7}$$

For convenience, one can represent the duty ratios with the following form:

$$d_k(t) = \frac{1 + d_0 + m_k(t)}{2},$$

$$d_{k+3}(t) = \frac{1 + d_0 - m_k(t)}{2}, \quad k = 1, 2, 3 \tag{4.8}$$

where $m_k(t)$, $k = 1, 2, 3$ is the time varying part of $d_k(t)$. Thus, from equation (4.2) to (4.7) one has

$$\frac{d}{dt}\begin{bmatrix} i_a \\ i_b \\ i_c \\ i_L \\ v_C \\ v_O \end{bmatrix} = \begin{bmatrix} \frac{-R_S}{L_S} & 0 & 0 & 0 & \frac{-m_1}{2L_S} & 0 \\ 0 & \frac{-R_S}{L_S} & 0 & 0 & \frac{-m_2}{2L_S} & 0 \\ 0 & 0 & \frac{-R_S}{L_S} & 0 & \frac{-m_2}{2L_S} & 0 \\ 0 & 0 & 0 & 0 & \frac{d_0}{L} & \frac{-1}{L} \\ \frac{m_1}{2C} & \frac{m_2}{2C} & \frac{m_3}{2C} & \frac{-d_0}{C} & 0 & 0 \\ 0 & 0 & 0 & \frac{1}{C_O} & 0 & \frac{-1}{RC_O} \end{bmatrix} \begin{bmatrix} i_a \\ i_b \\ i_c \\ i_L \\ v_C \\ v_O \end{bmatrix} + \frac{1}{L_S}\begin{bmatrix} e_a \\ e_b \\ e_c \\ 0 \\ 0 \\ 0 \end{bmatrix} \tag{4.9}$$

Next, assume that

$$\begin{aligned} e_a &= E_m \cos \omega t & i_a &= I_m \cos(\omega t - \phi) \\ e_b &= E_m \cos(\omega t - 120^0) & i_b &= I_m \cos(\omega t - 120^0 - \phi) \\ e_c &= E_m \cos(\omega t + 120^0) & i_c &= I_m \cos(\omega t + 120^0 - \phi) \end{aligned} \tag{4.10}$$

where for generality a phase shift ϕ is included in the line currents. It follows from equations (4.9) and (4.10) that one can obtain the following closed form solution

$$\begin{aligned} \frac{m_1(t)}{2} &= \frac{1}{v_C}[E_m \cos \omega t - R_S I_m \cos(\omega t - \phi) + \omega L_S I_m \sin(\omega t - \phi)] \\ &\equiv d_m \cos(\omega t - \psi) \\ \frac{m_k(t)}{2} &= d_m \cos(\omega t - \psi - (k-1)120^0), \quad k = 1, 2, 3 \end{aligned} \tag{4.11}$$

where

$$\begin{aligned} d_m &\equiv \frac{1}{v_C}\sqrt{(E_m - R_S I_m \cos\phi - \omega L_S I_m \sin\phi)^2 + (R_S I_m \sin\phi - \omega L_S I_m \cos\phi)^2} \\ \psi &\equiv \tan^{-1}\frac{\omega L_S I_m \cos\phi - R_S I_m \sin\phi}{E_m - R_S I_m \cos\phi - \omega L_S I_m \sin\phi} \end{aligned} \tag{4.12}$$

Next, define the following space vectors

$$
\begin{aligned}
\overset{\times}{e}_S &= \sqrt{\frac{2}{3}}\,(e_a + ae_b + a^2 e_c) \equiv (e_d + je_q)e^{jwt} \\
\overset{\times}{i}_S &= \sqrt{\frac{2}{3}}\,(i_a + ai_b + a^2 i_c) \equiv (i_d + ji_q)e^{jwt} \\
\overset{\times}{d}_S &= \sqrt{\frac{2}{3}}\,(d_1 + ad_2 + a^2 d_3) \equiv (d_d + jd_q)e^{jwt}
\end{aligned}
\tag{4.13}
$$

where $a = e^{j\frac{2}{3}p}$. It follows from equation (4.9) to (4.13) that

$$
\begin{aligned}
\frac{d}{dt}\overset{\times}{i}_S &= -\frac{R_S}{L_S}\overset{\times}{i}_S - \frac{v_C}{L_S}\overset{\times}{d}_S + \frac{1}{L_S}\overset{\times}{e}_S \\
\frac{d}{dt}i_L &= \frac{d_0}{L}v_C - \frac{1}{L}v_O \\
\frac{d}{dt}v_C &= \frac{1}{C}\mathrm{Re}[\overset{\times}{i}_S\ \overset{\times}{d}_S{}^*] - \frac{d_0}{C}i_L \\
\frac{d}{dt}v_O &= \frac{1}{C_O}i_L - \frac{1}{RC_O}v_O
\end{aligned}
\tag{4.14}
$$

Thus, by applying perturbation and linearization processes to equation (4.14) one can obtain the following DC model

$$
\begin{aligned}
&-E_d + R_S I_d - \boldsymbol{w} L_S I_q + D_d V_C = 0 \\
&-E_q + R_S I_q + \boldsymbol{w} L_S I_d + D_q V_C = 0 \\
&-D_0 V_C + V_O = 0 \\
&-D_d I_d - D_q I_q + D_0 I_L = 0 \\
&-I_L + \frac{V_O}{R} = 0
\end{aligned}
\tag{4.15}
$$

and the following small signal model

$$\frac{d}{dt}\begin{bmatrix}\hat{i}_d\\ \hat{i}_q\\ \hat{i}_L\\ \hat{v}_C\\ \hat{v}_O\end{bmatrix}=\begin{bmatrix}\frac{-R_S}{L_S} & \omega & 0 & \frac{-D_d}{L_S} & 0\\ -\omega & \frac{-R_S}{L_S} & 0 & \frac{-D_q}{L_S} & 0\\ 0 & 0 & 0 & \frac{D_0}{L} & \frac{-1}{L}\\ \frac{D_d}{C} & \frac{D_q}{C} & \frac{-D_0}{C} & 0 & 0\\ 0 & 0 & \frac{-1}{C_O} & 0 & \frac{-1}{RC_O}\end{bmatrix}\begin{bmatrix}\hat{i}_d\\ \hat{i}_q\\ \hat{i}_L\\ \hat{v}_C\\ \hat{v}_O\end{bmatrix}+\begin{bmatrix}\frac{-V_C}{L_S} & 0 & 0\\ 0 & \frac{-V_C}{L_S} & 0\\ 0 & 0 & \frac{V_C}{L}\\ \frac{I_d}{C} & \frac{I_q}{C} & \frac{-I_L}{C}\\ 0 & 0 & 0\end{bmatrix}\begin{bmatrix}\hat{d}_d\\ \hat{d}_q\\ \hat{d}_0\end{bmatrix}+\begin{bmatrix}\frac{1}{L_S} & 0\\ 0 & \frac{1}{L_S}\\ 0 & 0\\ 0 & 0\\ \end{bmatrix}\begin{bmatrix}\hat{e}_d\\ \hat{e}_q\end{bmatrix} \tag{4.16}$$

where

$$\begin{aligned} i_d &= I_d + \hat{i}_d & d_d &= D_d + \hat{d}_d\\ i_q &= I_q + \hat{i}_q & d_q &= D_q + \hat{d}_q\\ i_L &= I_L + \hat{i}_L & d_0 &= D_0 + \hat{d}_0\\ v_C &= V_C + \hat{v}_C & e_d &= E_d + \hat{e}_d\\ v_O &= V_O + \hat{v}_O & e_q &= E_q + \hat{e}_q \end{aligned}$$

Figs. 4.3 and 4.4 also show the corresponding equivalent circuits by using the ideal transformer model, which is also valid for DC quantities. These equivalent circuits are very useful for computer simulation and feedback controller design. Finally, it is worth deriving the output voltage gain. Substituting equations (4.10) and (4.11) into the first equation of (4.9) and separating the $\sin \omega t$ terms and $\cos \omega t$ terms yields the following two equations:

$$I_m = \frac{d_m \sin \delta}{\omega L_S \cos(\phi) - R_s \sin \phi} V_C \tag{4.17}$$

$$I_m = \frac{E_m - V_C d_m \cos \delta}{\omega L_S \sin(\phi) + R_s \cos \phi} \tag{4.18}$$

Then by substituting I_m of equation (4.17) into (4.18) and let $\phi = 0$, one can get the

desired voltage gain

$$\frac{V_O}{E_m} = \frac{d_m}{d_0}\frac{R_S \sin \boldsymbol{j} + \boldsymbol{w} L_S \cos \boldsymbol{j}}{\boldsymbol{w} L_S} \tag{4.19}$$

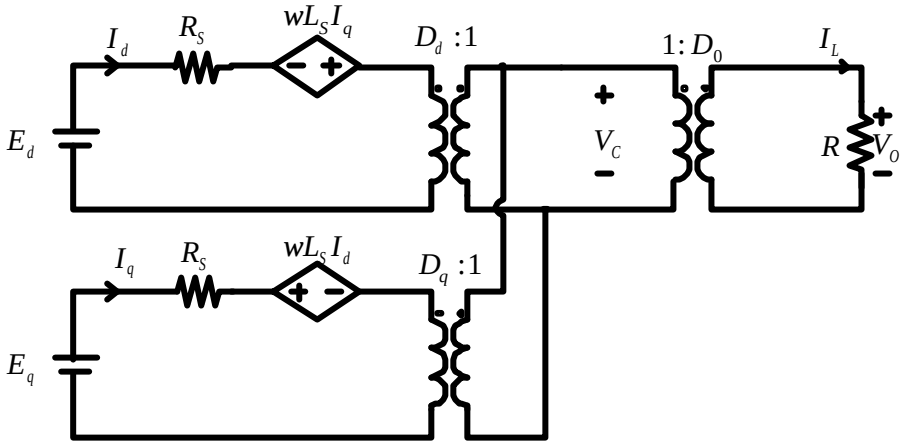

Fig. 4.3 Equivalent DC circuit model of the converter

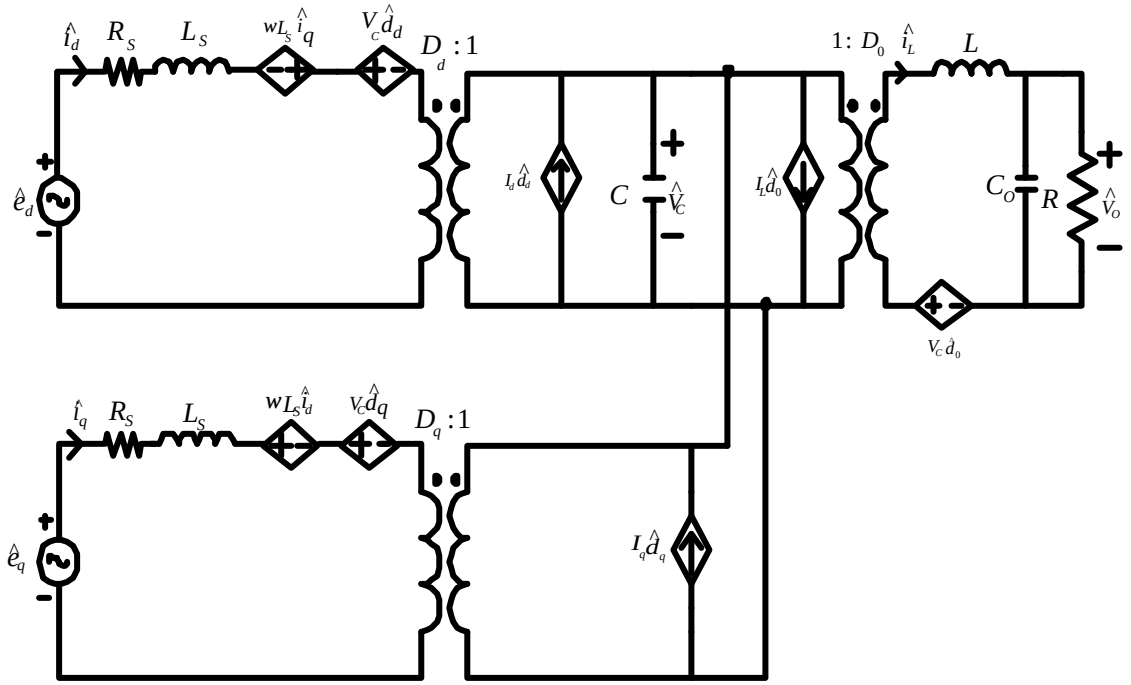

Fig. 4.4 Equivalent AC circuit model of the converter

4.4 The Proposed Maximum Constant D_0 Controller

From the previous closed form duty ratio solution of the corresponding switches, it is seen that a constant duty ratio solution of $D_7 = 1 - D_0$ for S_7 does exist. Also, from equation (4.15) one can see that, for a fixed V_O, larger D_0 will result in lower V_C for capacitor C. The remaining problem is how to implement the PWM control in the previous section. From equations (4.8) and (4.11)

$$\begin{aligned} d_k(t) &= \frac{1+d_0}{2} + \frac{m_k(t)}{2} \\ &= \frac{1+d_0}{2} + d_m \cos(\omega t - \phi - (k-1)120^0), \\ d_{k+3}(t) &= \frac{1+d_0}{2} - d_m \cos(\omega t - \phi - (k-1)120^0) \\ & \qquad\qquad k = 1, 2, 3 \end{aligned} \tag{4.20}$$

Thus, it is required that

$$0 < d_0 \le 1 - 2d_m \tag{4.21}$$

to achieve the ideal converter characteristic, namely sinusoidal line current and clean DC output. On the other hand, from three-phase boost rectifier operation principle, it is known that only during the periods of $d_{01}T_S$ and $d_{02}T_S$ as defined in Fig. 4.2 there is no energy transfer from the ac subcircuit to the output dc subcircuit. Hence, based on this fact and concerning the implementation of constant D_0 control for the proposed converter, one can first identify the switch status corresponding to $(d_2 - \frac{d_0}{2})T_S$ $((d_6 - \frac{d_0}{2})T_S)$ in Fig. 4.2 where S_1, S_2 and S_3 (S_4, S_5, and S_6)

are all turned on. Then, partition a portion defined as $\frac{1}{2}d_0 T_S$ in Fig. 4.2, to turn on the remaining three switches. In other words, during these two portions, all six bridge switches are turned on and S_7 is turned off. The remaining question is how to achieve maximum d_0 control.

Define

$$\begin{aligned} d_a(t) &\equiv \frac{1}{2} + d_m \cos(\omega t - \phi) \\ d_b(t) &\equiv \frac{1}{2} + d_m \cos(\omega t - \phi - 120^0) \\ d_c(t) &\equiv \frac{1}{2} + d_m \cos(\omega t - \phi + 120^0) \end{aligned} \tag{4.22}$$

Then, in order to achieve the ideal performance without distortion, one can choose

$$\begin{aligned} \frac{1}{2}D_0 &= \min_t \{d_a(t),\ d_b(t),\ d_c(t)\} \\ &= \frac{1}{2} - d_m \end{aligned} \quad , \tag{4.23}$$

for the time interval where S_1, S_2 and S_3 are all closed. Similarly, one can choose the other half D_0 from the interval where S_4, S_5 and S_6 are all closed:

$$\begin{aligned} \frac{1}{2}D_0 &= \min_t \{(1-d_a(t)), (1-d_b(t)), (1-d_c(t))\} \\ &= \frac{1}{2} - d_m \end{aligned} \tag{4.24}$$

It follows from equations (4.23) and (4.24) that

$$D_0 = 1 - 2d_m . \tag{4.25}$$

Thus, from inequality equation (4.21) one can see that the maximum duty ratio can indeed be achieved. It follows from equation (4.12) that under maximum d_0 control

one has

$$\begin{aligned} V_C - V_O &= (1 - D_0)V_C \\ &= 2d_m V_C \\ &= 2\sqrt{(E_m - R_S I_m \cos f - wL_S I_m \sin f)^2 + (R_S I_m \sin f - wL_S I_m \cos f)^2} \end{aligned} \tag{4.26}$$

Thus, from equation (4.26) one can see that, under maximum d_0 control and for a fixed output power (or fixed I_m and f), $V_C - V_O$ is constant. As an illustration, consider a three-phase 220 V(rms) ac source, $pf = 1.0$, $R_S = 0.45\,\Omega$, $L = 7.5\,mH$, $P_O = 3kW$ and V_O is adjustable from $50\,V$ to $500\,V$. Then, for a fixed qualified d_0 control ($d_0 = 0.1$), capacitor voltage V_C is varied from $500V$ to $5000V$. However, for the proposed maximum d_0 control (D_0 is varied from 0.1235 to 0.5849), V_C is changed from $405V$ to $855V$ only. Therefore, from the viewpoint of the practical applications, especially for wide step up/down adjustable range applications, the proposed maximum D_0 control is indeed essential. Based on the previous theoretical basis, Fig. 4.5 shows an implementation block diagram for $pf = 1.0$ as an example. From Fig. 4.5 one can see that ac line current amplitude (I_m) is generated through closed loop control of V_O. From conservation of power one knows that if $V_O = V_{O,ref}$ then I_m will be the correct one automatically. Hence, it is not necessary to use a current sensor. Similarly, a small three-phase rectifier is adopted to generate the desired d_m signal through closed-loop control. Fig. 4.6 and Fig. 4.7 show the detailed implementation of both switch signal generators for the six

bridge switches. Finally, S_7 is open only when all six bridge switches are turned on.

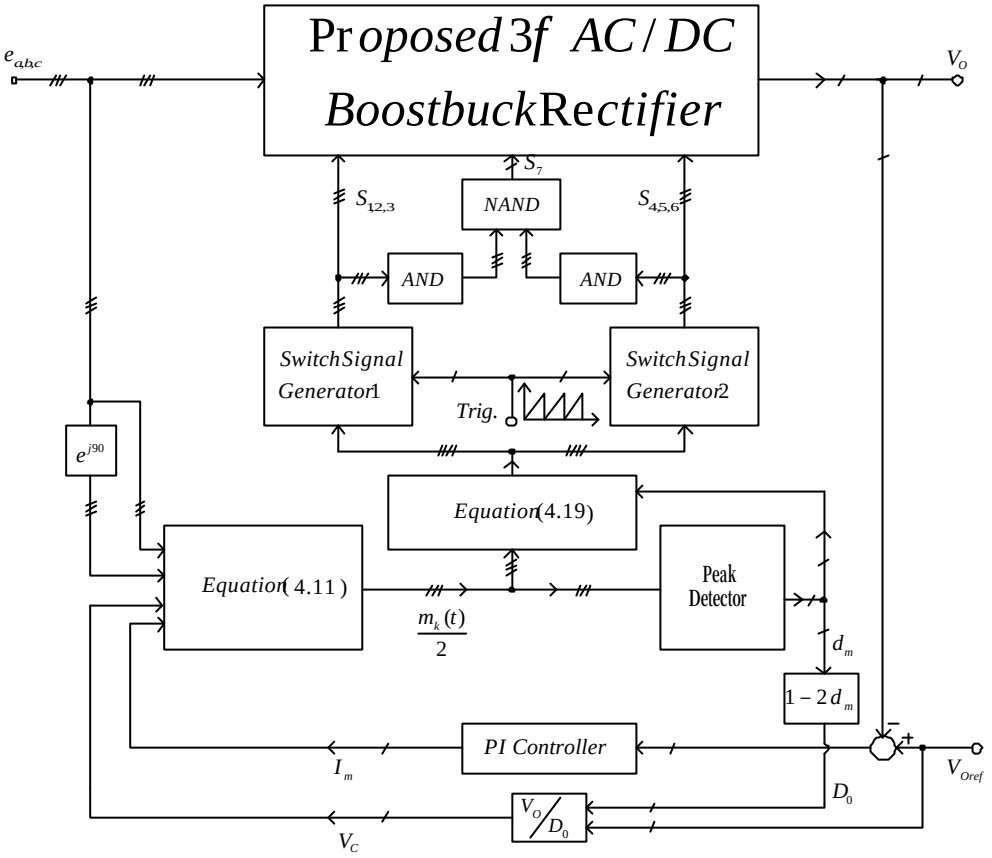

Fig. 4.5 An implementation block diagram of the proposed controller

4.5 Some Experimental Results

As an illustrative example, consider the following converter parameters

$$R_S = 0.45\,\Omega,\quad L_S = 7.5\,mH,\quad pf = 1.0$$

$$L = 7.5\,mH,\quad C = 1500\,mF,\quad f_S = 4\,kHz$$

$$C_O = 1500\,mF,\quad P_O = V_O^2 / R = 500\,W.$$

Also, due to the constraint of the laboratory limitation, assume

$$e_a(t) = 50\sqrt{\frac{2}{3}}\cos(\omega t) \quad V$$

$$e_b(t) = 50\sqrt{\frac{2}{3}}\cos(\omega t - 120^0) \quad V$$

$$e_c(t) = 50\sqrt{\frac{2}{3}}\cos(\omega t + 120^0) \quad V\,.$$

Hence, $E_m = 40.82\ V$. From the DC model and with constant $P_O = 500\ W$, Fig. 4.8 shows the voltage gain V_O/E_m of equation (4.19) with respect to modulation index d_m and modulation angle $\jmath$. Also, the converter can indeed function as a step-up as well as a step down converter.

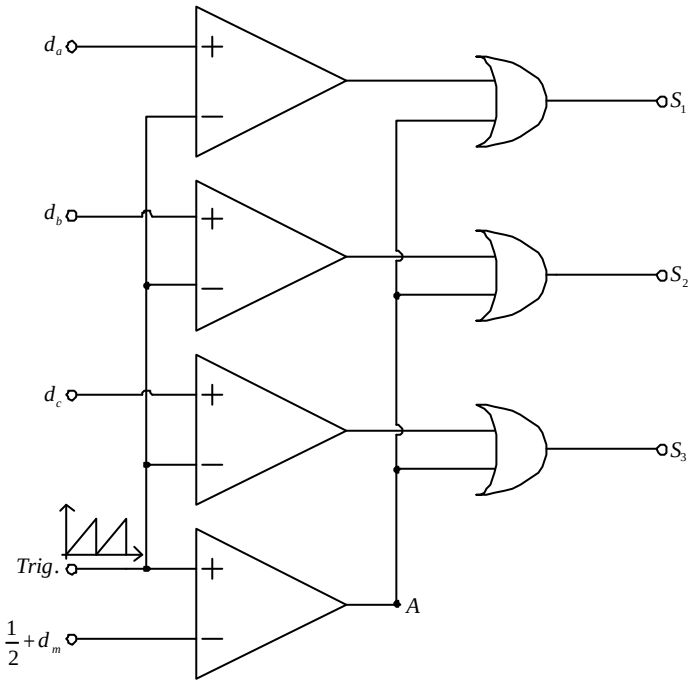

(a)

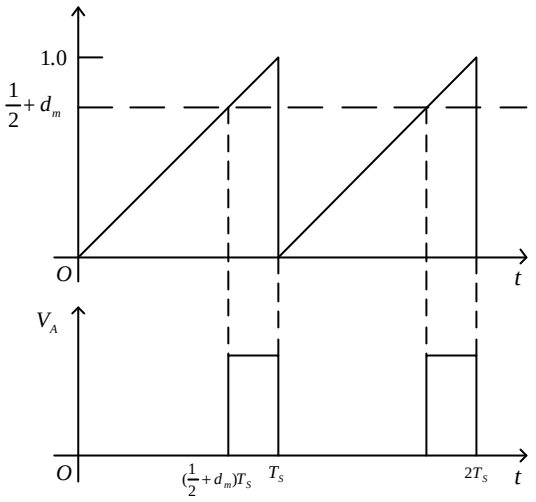

(b)

Fig. 4.6 Schematic diagram of first switch signal generator (a) Generation for S_1, S_2 and S_3 signals, (b) Generating of $\frac{1}{2}D_0T_S$

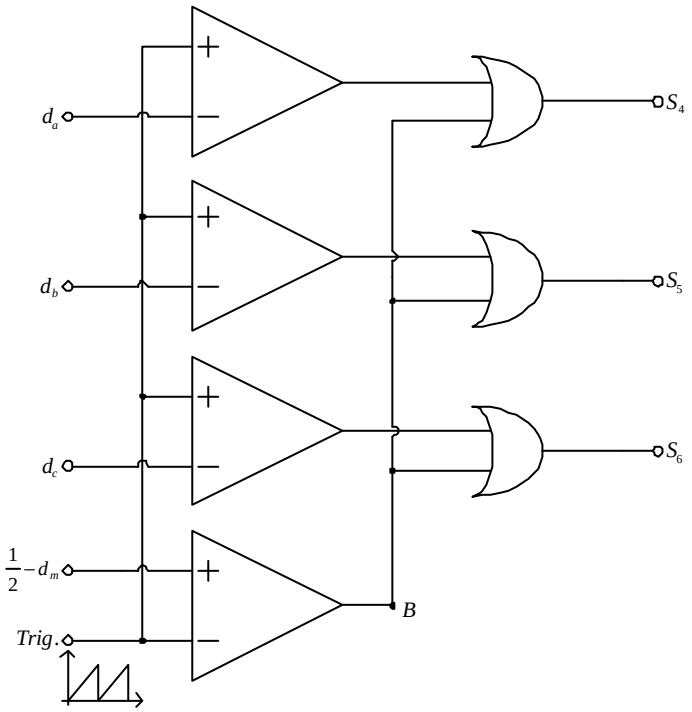

(a)

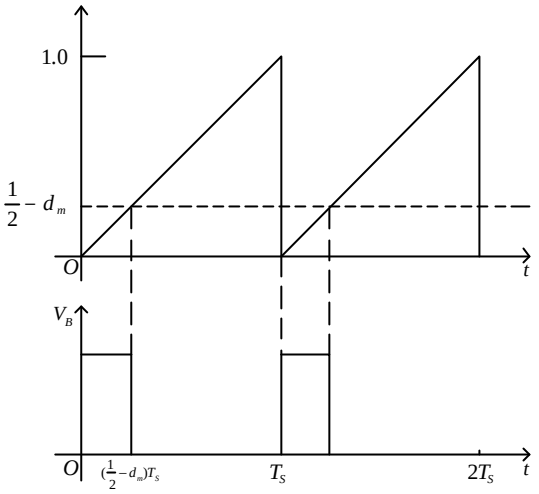

(b)

Fig. 4.7 Schematic diagram of second switch signal generator (a) Generation for S_4, S_5 and S_6 signals, (b) Generating of $\frac{1}{2} D_0 T_S$

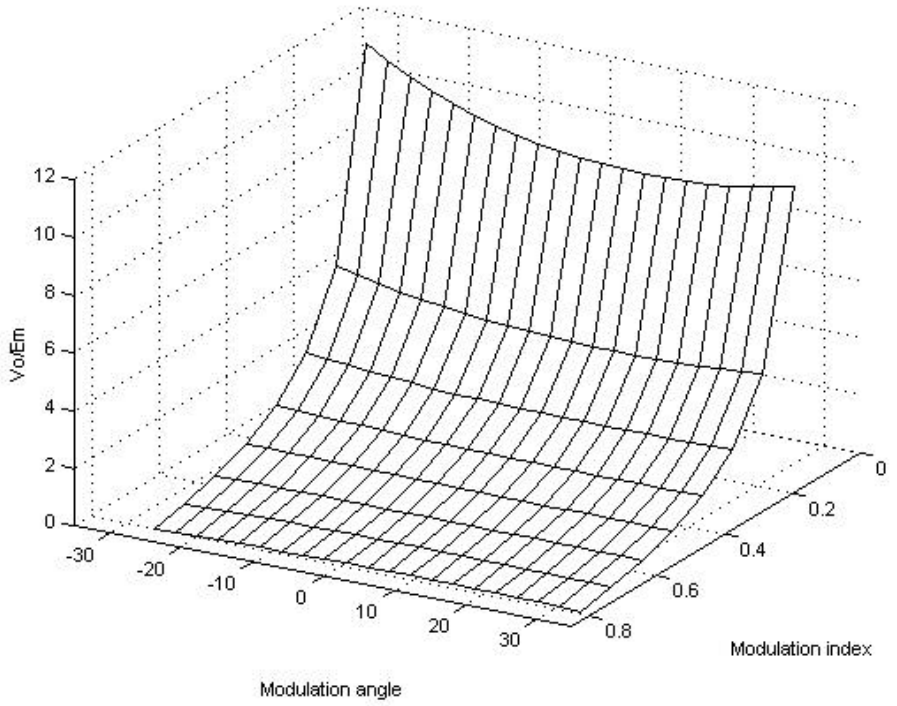

Fig. 4.8 The output voltage gain as a function of modulation index d_m and modulation angle j.

Next consider the step-down case with $V_O = 20\,V$ and $P_O = 500\,W$. Fig. 4.9 shows the measured waveforms of e_a and i_a as well as the measured waveforms of V_O and V_C.

From Fig. 4.9 one can see that the measured results are as expected from the previous theoretical basis. Fig. 4.10 also shows the measured results of the gating signal of S_7 and the current waveform of i_L for reference. From Fig. 4.10 one can see that the maximum D_0 is equal to 0.18 approximately. Also, from Fig. 4.10 (b) one can see that the waveform of i_L agrees with Fig. 4.10(a) very well. In other words, the inductor current i_L is decreasing during $d_7 T_S$ and is increasing during $D_0 T_S$ while charging by V_C.

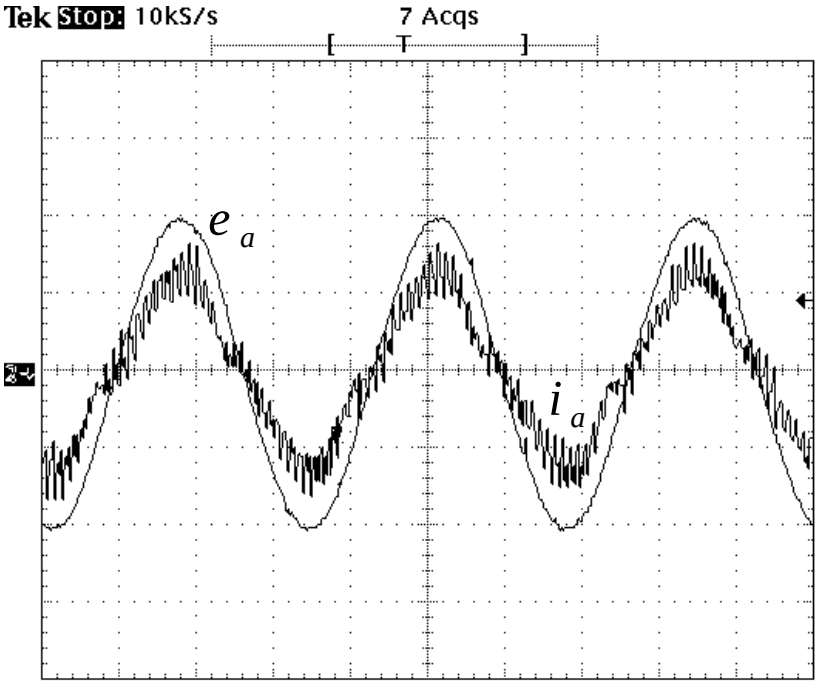

(a)

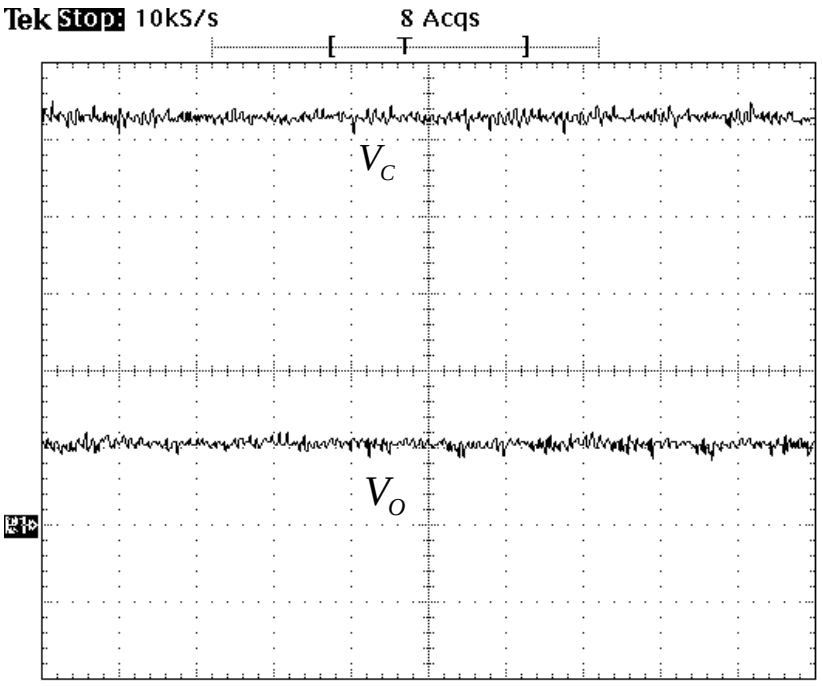

(b)

Fig. 4.9 Measured waveforms of (a) e_a and i_a (e_a: 20v/div, i_a: 8a/div, 5msec/div), (b) V_O and V_C (20v/div) under step down operation

Third, consider the step-up case with $V_O = 90\,V$ and $P_O = 500\,W$. It is worth mentioning that to the author's best knowledge, so far there is no clear definition about step-up or step-down of three-phase AC/DC converters. Fortunately, the proposed maximum constant D_0 control, D_0=0.5 can be used to define the step up/down cases. More precisely, for $D_0 = \frac{1}{2}$, then

$$V_O = 2\sqrt{(E_m - R_S I_m \cos(\boldsymbol{f}) - \boldsymbol{w} L_S I_m \sin(\boldsymbol{f}))^2 + (\boldsymbol{w} L_S I_m \cos(\boldsymbol{f}) - R_S I_m \sin(\boldsymbol{f}))^2}$$
$$\equiv 2V_{base}$$

Therefore, when $D_0 > \frac{1}{2}$ for the maximum constant D_0 control, then $V_O > 2V_{base}$

and is called step-up case. Similarly, for $D_0 < \frac{1}{2}$, then $V_O < 2V_{base}$ and is called step-down case. This agrees with the definition of the C'uk DC/DC converter.

Fig. 4.11 shows the measured waveforms of e_a and i_a as well as the measured waveforms of V_O and V_C for the step-up case.

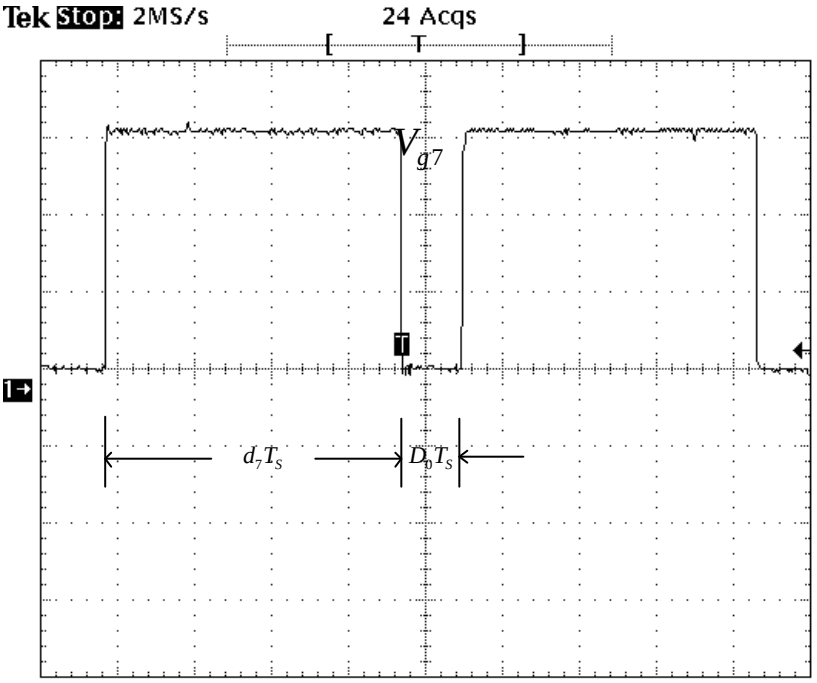

(a)

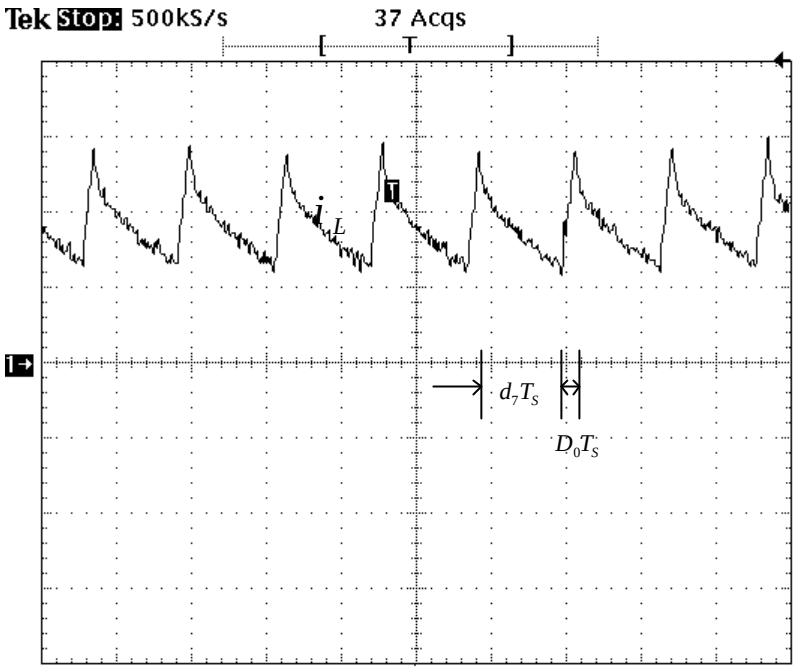

(b)

Fig. 4.10 Measured waveforms of (a) the gating signal of S_7 (2v/div, 0.05ms/div), (b) inductor current i_L (15a/div, 0.2ms/div) under step down operation

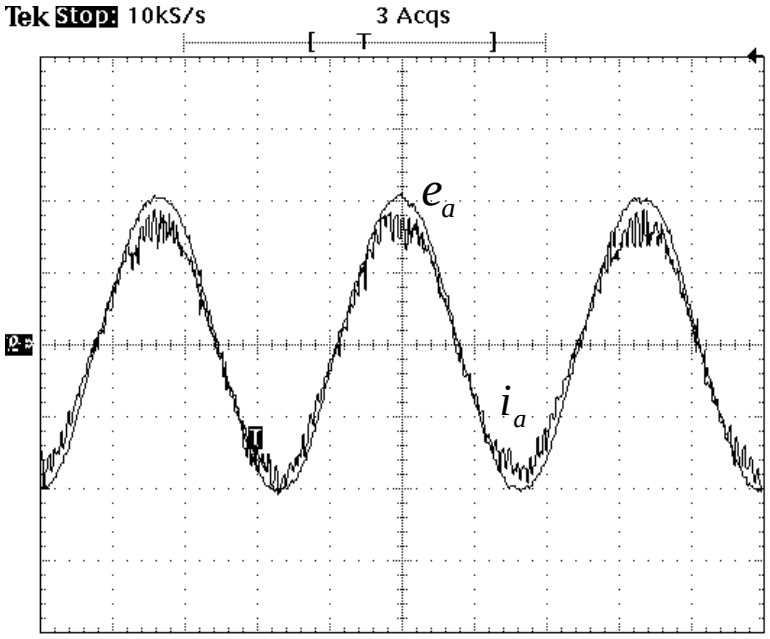

(a)

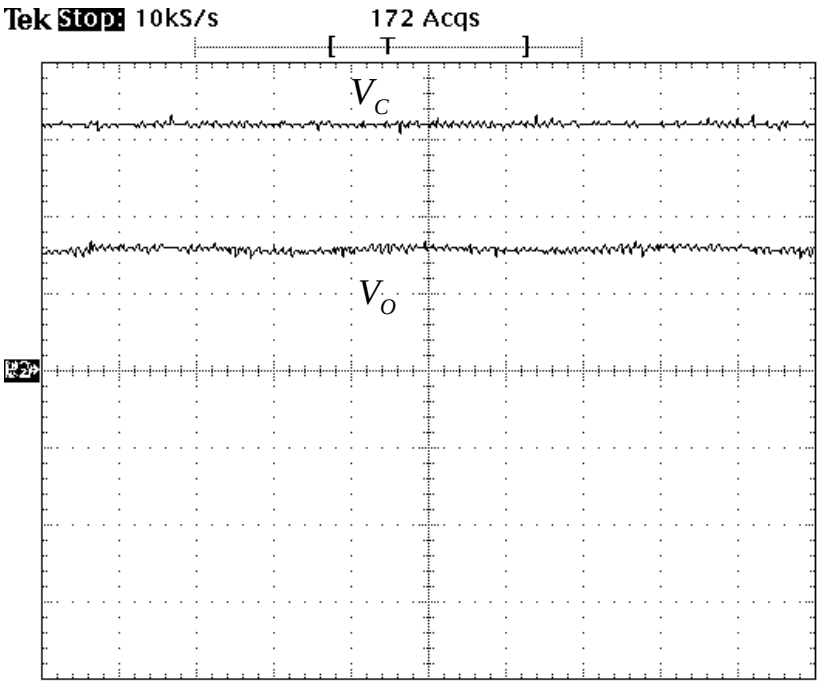

(b)

Fig. 4.11 Measured waveforms of (a) e_a and i_a (e_a: 20v/div, i_a: 5a/div, 5msec/div), (b) V_O and V_C (60v/div) under step up operation

Fig. 4.12 also shows the measured gating signal of S_7 and the measured waveform of $i_L(t)$. From Fig. 4.12 one can see that $D_0 = 0.51$ which means the step-up case and that $i_L(t)$ increases and decreases during D_0T_S and d_7T_S, respectively.

Finally, the output resistance load is paralleled with a 30V DC source in series with a 1Ω resistance and a switch for testing the regeneration case. Fig. 4.13 shows the measured waveforms of e_a and i_a for $V_O = 20\,V$. From Fig. 4.13 one can see that the proposed converter indeed possesses the regenerative capability.

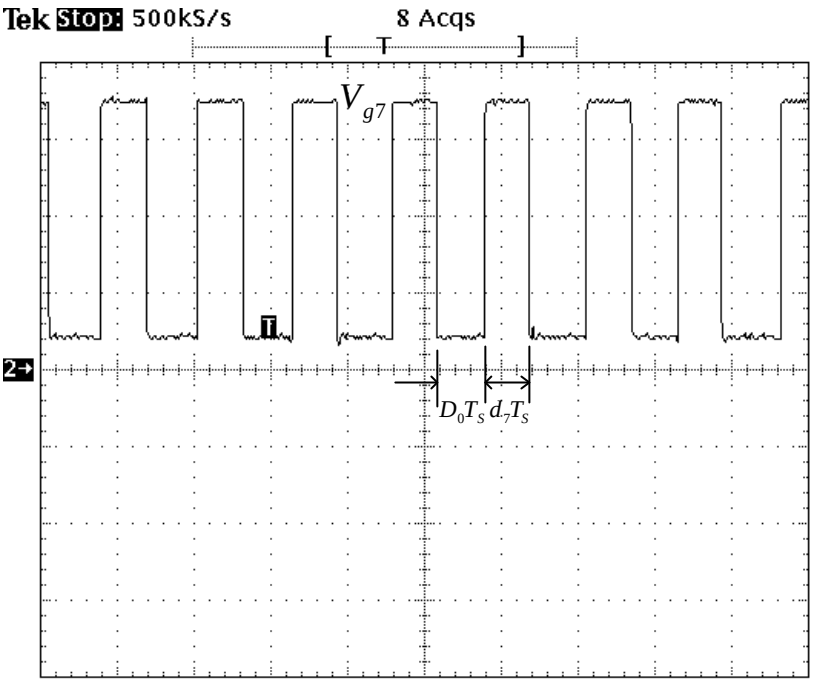

(a)

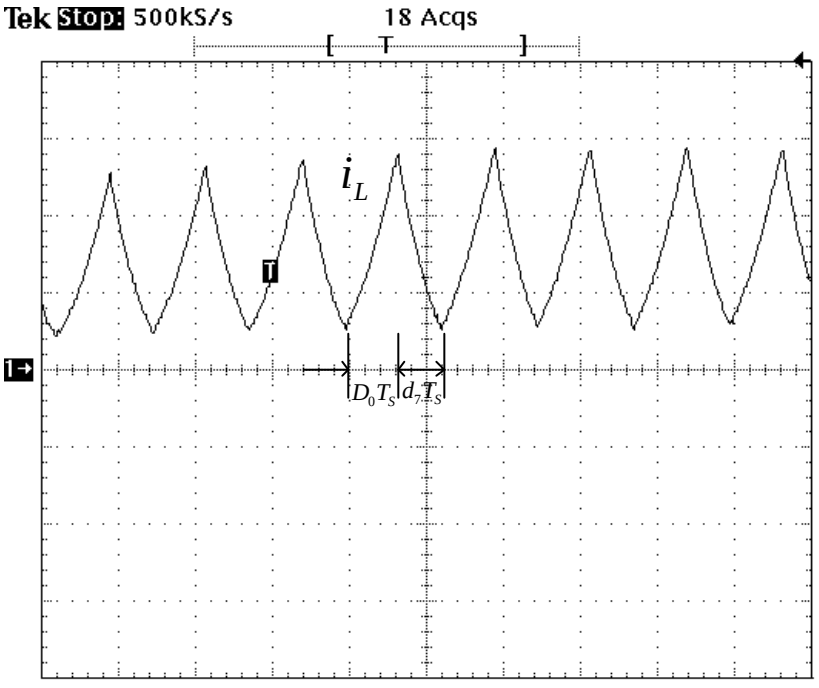

(b)

Fig. 4.12 Measured waveforms of (a) the gating signal of S_7 (2v/div, 0.2ms/div), (b) inductor current i_L (3a/div, 0.2ms/div) under step up operation

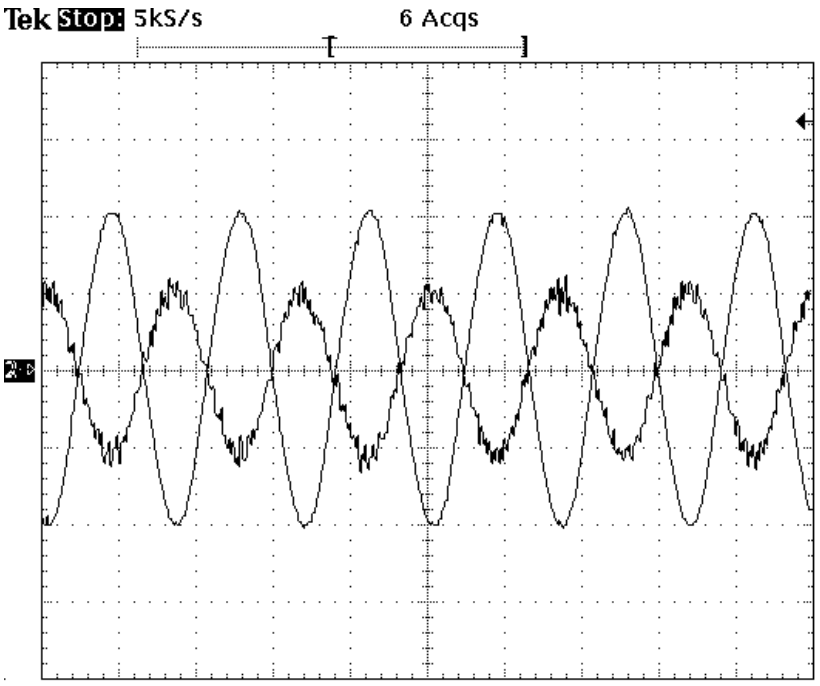

Fig. 4.13 Measured waveforms of e_a and i_a under regeneration mode

(e_a : 20v/div, i_a : 5a/div, 5msec/div)